HAL
open science

Liraglutide improves hepatic steatosis and metabolic dysfunctions in a 3-week dietary mouse model of nonalcoholic steatohepatitis

Thibaut Duparc, François Briand, Charlotte Trenteseaux, Jules Merian, Guillaume Combes, Souad Najib, Thierry Sulpice, Laurent O. Martinez

▶ To cite this version:

Thibaut Duparc, François Briand, Charlotte Trenteseaux, Jules Merian, Guillaume Combes, et al.. Liraglutide improves hepatic steatosis and metabolic dysfunctions in a 3-week dietary mouse model of nonalcoholic steatohepatitis: Liraglutide efficacy in a novel NASH model. AJP - Gastrointestinal and Liver Physiology, 2019, 317 (4), pp.G508-G517. 10.1152/ajpgi.00139.2019 . inserm-02569247

HAL Id: inserm-02569247

https://inserm.hal.science/inserm-02569247

Submitted on 11 May 2020

HAL is a multi-disciplinary open access archive for the deposit and dissemination of scientific research documents, whether they are published or not. The documents may come from teaching and research institutions in France or abroad, or from public or private research centers.

L'archive ouverte pluridisciplinaire **HAL**, est destinée au dépôt et à la diffusion de documents scientifiques de niveau recherche, publiés ou non, émanant des établissements d'enseignement et de recherche français ou étrangers, des laboratoires publics ou privés.

HAL
archives-ouvertes.fr

Liraglutide improves hepatic steatosis and metabolic dysfunctions in a 3-week dietary mouse model of non-alcoholic steatohepatitis. Short title: Liraglutide efficacy in a novel NASH model

Thibaut Duparc, François Briand, Charlotte Trenteseaux, Souad Najib, Thierry Sulpice, Laurent Martinez

To cite this version:

Thibaut Duparc, François Briand, Charlotte Trenteseaux, Souad Najib, Thierry Sulpice, et al.. Liraglutide improves hepatic steatosis and metabolic dysfunctions in a 3-week dietary mouse model of non-alcoholic steatohepatitis. Short title: Liraglutide efficacy in a novel NASH model. AJP - Gastrointestinal and Liver Physiology, American Physiological Society, 2019. inserm-02569247

HAL Id: inserm-02569247

https://www.hal.inserm.fr/inserm-02569247

Submitted on 11 May 2020

HAL is a multi-disciplinary open access archive for the deposit and dissemination of scientific research documents, whether they are published or not. The documents may come from teaching and research institutions in France or abroad, or from public or private research centers.

L'archive ouverte pluridisciplinaire **HAL**, est destinée au dépôt et à la diffusion de documents scientifiques de niveau recherche, publiés ou non, émanant des établissements d'enseignement et de recherche français ou étrangers, des laboratoires publics ou privés.

Liraglutide improves hepatic steatosis and metabolic dysfunctions in a 3-week dietary mouse model of non-alcoholic steatohepatitis.

Short title: Liraglutide efficacy in a novel NASH model

Thibaut Duparc [1], François Briand [2], Charlotte Trenteseaux [3], Jules Merian [1], Guillaume Combes [1], Souad Najib [1], Thierry Sulpice [2], Laurent O. Martinez [1]

[1] Inserm, Université de Toulouse, UMR1048, Institute of Metabolic and Cardiovascular Diseases (I2MC), Toulouse, France.

[2] Physiogenex SAS, Prologue Biotech, 516 Rue Pierre et Marie Curie, 31670 Labège-Innopole, France.

[3] Lifesearch SAS, 195 Route d'Espagne, 31036 Toulouse Cedex 1, France.

T.D, F.B, T.S and L.O.M designed research; T.D, F.B, L.O.M and S.N analyzed data; G.C, T.D, J.M and C.T performed research; T.D and L.O.M wrote the paper. All authors read and approved the final manuscript.

Corresponding author: T. Duparc, INSERM UMR1048, Bât. L3, Hôpital Rangueil, BP 84225, 31432 Toulouse cedex 04, France. Tel: +33 (0)5 31 22 40 82. Email: thibaut.duparc@inserm.fr

ABSTRACT

Aim: Non-alcoholic steatohepatitis (NASH) is an emerging health problem worldwide. However, efficacious pharmacological treatment for NASH is lacking. A major issue for preclinical evaluation of potential therapeutics for NASH is the limited number of appropriate animal models, i.e., models that do not require long-term dietary intervention and adequately mimic disease progression in humans. The present study aimed to evaluate a 3-wk dietary mouse model of NASH and to validate it by studying the effects of liraglutide, a compound in advanced clinical development for NASH.

Methods: C57BL6/J mice were fed a diet high in fat (60%), cholesterol (1.25%) and cholic acid (0.5%) along with 2% hydroxypropyl-β-cyclodextrin in drinking water (HFCC-CDX diet). Histological and biological parameters were measured at 1 and 3 wk. After 1-wk diet induction, liraglutide was administrated daily for 2 wk, and then NASH-associated phenotypic aspects were evaluated in comparison with control mice.

Results: Prior to treatment with liraglutide, mice fed the HFCC-CDX diet for 1 wk developed liver steatosis and had increased levels of oxidative-stress markers and hepatic and systemic inflammation. For mice not treated with liraglutide, these aspects were even more pronounced after 3 wk of the dietary period, with additional liver insulin resistance and fibrosis. Liraglutide treatment corrected the diet-induced alterations in glucose metabolism and significantly reduced hepatic steatosis and inflammation.

Conclusion: This study provides a novel 3-wk dietary model of mice that rapidly develop NASH features, and this model will be suitable for evaluating the therapeutic efficacy of compounds in preclinical drug development for NASH.

Keywords: Dietary model, Drug development, Dyslipidemia, Nonalcoholic fatty liver disease, Nonalcoholic steatohepatitis

New & Noteworthy: We propose a diet high in fat (60%), cholesterol (1.25%), and cholic acid (0.5%) along with 2% hydroxypropyl--cyclodextrin in drinking water (HFCC-CDX diet) as a new dietary model of nonalcoholic steatohepatitis. We used the HFCCCDX model to reproduce the main features of disease development in humans for the purpose of facilitating the rapid screening of drug candidates

and prioritizing the more promising candidates for advanced preclinical assessment and subsequent clinical trials

1 - INTRODUCTION

Non-alcoholic fatty liver disease (NAFLD) is a chronic disease that has become pandemic, as it affects between 20% and 30% of the general adult population of most Westernized countries.

Although most cases of NAFLD follow a benign course, approximatively 20% evolve into an aggressive form termed nonalcoholic steatohepatitis (NASH), in which inflammation in the liver can cause hepatocyte damage with or without fibrosis (9). NASH typically entails high levels of hepatic lipid peroxidation, oxidative stress, apoptosis and production of proinflammatory and profibrotic cytokines that induce necroinflammation and ultimately fibrosis (1, 14). Progressive evolution of hepatic inflammation and fibrosis can lead to cirrhosis, liver failure or hepatocellular carcinoma, with end-stage liver disease due to NASH being anticipated as the leading indication for liver transplantation in subsequent years (4, 22). Generally, pathogenic drivers and rates of progression of NAFLD are not identical among all patients; thus, NASH should not be thought of as an orderly progression of stages. Although certain advances have led to a better understanding of the pathogenesis of NAFLD and to the identification of therapeutic targets and drugs, no therapy for NASH exists other than lifestyle modifications (to ensure weight loss) and bariatric surgery for morbidly obese patients (6, 34).

Although drug development for NASH has accelerated in recent years, the choice of animal models remains one of the major issues for the assessment of drug candidates at the initial steps of preclinical development. Indeed, an appropriate animal model should recreate as closely as possible the pathological patterns, metabolic and transcriptomic features, and histological alterations found in human NASH. Several preclinical mouse and rat models for NASH are currently available, with various approaches based on genetic modification, e.g., ob^{-}/ob^{-} or db^{-}/db^{-} mice with leptin and leptin receptor deficiency, respectively, diet induction, e.g., high-fat/cholesterol/fructose diet or methionine/choline–deficient diet, or chemical induction, e.g., thioacetamide or carbon tetrachloride (14, 20, 27, 30). Each of these models can be used separately or in combination. Although these models are mandatory tools for assessing the efficacy of candidate compounds before proceeding to clinical trials, the majority do not entirely replicate human NASH features, i.e., they may lack fibrosis or lack insulin resistance in diet-induced models (26). Another important issue that may hinder preclinical assessment of NASH drug candidates is the large amount of resources and time needed to bring a model to a standard suitable for experimental studies, as most of the existing models require several

weeks, ranging from 6 - 40 wk, to create a NASH phenotype (14). Hence, there is need for animal models that rapidly develop NASH features and recapitulate the human pathology as accurately as possible, which would permit an initial, economical, and rapid preclinical evaluation of drug candidates. To address the issues associated with current NASH models, we developed, characterized, and evaluated the utility of a rapid-onset and inexpensive murine model of NASH based on dietary induction. Toward this goal, we customized a high-fat diet (60% of calories) containing high levels of cholesterol (1.25%) and cholic acid (0.5%), components that have been used separately or in combination to promote hepatic steatosis and lipotoxicity (8, 25, 37). To promote cholesterol uptake by the liver, we also supplemented the drinking water with 2% hydroxypropyl-β-cyclodextrin (CDX), a cyclic oligosaccharide that has high affinity for sterols (7). Beginning at age 8 wk, C57BL/6J mice were fed this high-fat, high-cholesterol, cholate and CDX (HFCC-CDX) diet for 1 or 3 wk, after which parameters related to hepatic steatosis, liver inflammation, liver fibrosis, and glucose metabolism were measured. In parallel, another group of experimental mice were fed the HFCC-CDX diet for 3 wk, but after 1 wk they were also treated daily with liraglutide, a GLP-1 analog currently in advance clinical development for NASH (2). These groups were then compared with respect to NASH phenotype.

2 - MATERIALS AND METHODS

2.1 - Animals, diets and drugs

All animal procedures were performed in accordance with the guidelines of the Committee on Animals of the Midi-Pyrénées Ethics Committee on Animal Experimentation and with the French Ministry of Agriculture license. Wild-type C57BL/6J male mice were caged in animal rooms with 12-h light/12-h dark cycle and *ad libitum* access to water and diet. One week before the initiation of the study, serum levels of alanine (ALT) and aspartate (AST) aminotransferases were measured in each mouse and homogenous groups of mice were constituted according to these transaminases levels. At the initiation of the dietary intervention, all animals were 8 weeks old and were fed a chow diet (V1534-000, Ssniff, Germany). During the experimental period, mice were provided with either the chow diet for 3 wk (CD control group) or a custom diet high in fat (60 kcal%), cholesterol (1.25%) and cholic acid (0.5%) (D11061901, Research Diet) as well as 2% CDX (Fisher Scientific) in drinking water (HFCC-CDX group).

For the last 2 wk of the 3-wk period, groups of mice fed the HFCC-CDX diet received a daily intraperitoneal injection of either liraglutide (Victoza, Novo Nordisk) at 100 µg/kg body wt or vehicle (phosphate-buffered saline).

2.2 - Liver histology

A sample of the main liver lobe was fixed with paraformaldehyde, embedded in paraffin, and sliced into 5-µm sections, then deparaffinized, rehydrated, and stained with Sirius Red or H&E to assess histopathology. For Sirius Red staining, sections were incubated for 10 min in 1% Sirius Red (Sigma) dissolved in saturated picric acid and then rinsed with distilled water. For H&E staining, sections were incubated for 30 min in Mayer hematoxylin solution, rinsed with distilled water for 5 min, and then incubated in saturated lithium carbonate solution for 15 s. Sections were then rinsed again with distilled water for 3 min, and finally placed in 0.5% alcoholic eosin solution for 30 s. Staining with Oil Red O (ORO) was performed on paraformaldehyde-fixed liver fractions, and sections were mounted in Cellpath™ OCT Embedding Matrix (Fisher Scientific, France). Samples were sliced in 7-µm thick sections and stained with 0.5% ORO solution in isopropanol for 15 min. The slides were transferred to a 60% isopropanol solution for 1 min, washed with distilled water, and processed for hematoxylin counter staining. For all staining procedures, sections were dehydrated for 15 min with absolute ethanol and incubated with Histoclear® clearing agent (Euromedex) before mounting with Distyrene Plasticizer Xylene and coverslipped. After being stained, slides were scanned with a NanoZoomer 2.0 RS (Hamamatsu, Japan) and then hepatocellular steatosis, liver inflammation and lobular fibrosis were blindly assessed by a histopathologist (Histalim, Montpellier, France) using a scoring method adapted from Kleiner *et al.* (19). More precisely, steatosis was scored as 0 (<5%), 1 (5-33%), 2 (33-66%), 3 (> 66%); lobular inflammation was scored as 0 (no foci), 1 (<2 foci per X200 field), 2 (2-4 foci per X200 field), or 3 (>4 foci per X200 field); and fibrosis was scored as 0 (none), 1 (perisinusoidal or periportal), 2 (perisinusoidal and periportal), 3 (bridging fibrosis), or 4 (cirrhosis). An individual NAFLD activity total score was then calculated for each animal by adding up the thre scores.

2.3 - Liver lipid content

Total lipids were measured in liver tissue after extraction with chloroform-to-methanol ratio (2:1) according to Folch *et al*.(12). Briefly, 100 mg liver tissue was homogenized in 900 µl phosphate buffer pH 7.4 until complete tissue lysis. Lipids were extracted by mixing 125 µl of each lysate with 1 ml chloroform-to-methanol ratio (2:1). After centrifugation, the chloroform phase was evaporated under

nitrogen, and the dried residue was solubilized in 200 µl isopropanol. Triglycerides and cholesterol were measured using commercial kits based on the CHOD-PAP and GPO-PAP detection methods (Biolabo SA, Maizy, France). Results are expressed as micrograms of lipid per milligram liver.

2.4 - Measuring liver reactive oxygen species and TBARS

Reactive oxygen species (ROS) in liver were assayed according to the protocol of Szabados *et al.* (31). Briefly, 30 mg of liver tissue was homogenized in a cold buffer (in mM : 150 KCl, 20 Tris-base, 0.5 EGTA, 1 $MgCl_2$, 5 glucose and 0.5 octanoic acid at pH 7.4). After complete tissue lysis and centrifugation at 12,000 *g*, the ROS-reactive fluorescent probe H_2-DCFDA (Molecular Probes) was added to each supernatant to yield 4 µM final concentration of probe, and samples were incubated at 37°C for 30 min with slight agitation. Then, 125 µl of 70% ethanol and 125 µl of 0.1 N HCl were added to stop the reaction. Samples were centrifuged at 3,000 *g* for 15 min at 4°C, and supernatants were collected in new tubes and neutralized by addition of 175 µl of 1 M $NaHCO_3$ solution. Each supernatant (200 µl) was added into a black 96-well plate (NUNC), and fluorescence was measured (485 nm excitation, 535 nm emission). Relative fluorescence units were normalized with protein content of each sample, and results are expressed as the percentage of fluorescence versus control.

To assess lipid peroxidation, thiobarbituric acid response substrates (TBARS), which are byproducts of lipid peroxidation, 200 µl of 0.6% TBA and 10 µl of 1% H_3PO_4 solutions were added to 100 µl of liver homogenate. Samples were incubated at 95°C for 1 h, followed by the addition of 200 µl of butanol, mixing, and centrifugation at 12,000 *g* to extract the colored phase. Fluorescence was measured (515 nm excitation, 548 nm emission), and the TBARS concentration was calculated in comparison with a standard curve. Results were normalized with the protein content of each sample and are expressed as nanomole per milligram of protein.

2.5 - RNA extraction and real-time quantitative PCR analysis

Total RNA was prepared from liver tissue using QIAzol lysis reagent (QIAGEN, Germantown, USA). Extracted RNAs were suspended in DNase/RNase-free water, and the concentration of each sample was calculated after measuring absorbance at 260 nm using a NanoDrop spectrophotometer (Thermo Scientific™, Waltham, USA). Reverse transcription of mRNA (1 µg) was performed using M-MLV Reverse Transcriptase (Promega, Madison, WI) in the presence of a random primer [oligo(dT), 2 µl, 500 µg/ml; Promega) and 0.5 µl RNaseOUT™ (ThermoFisher scientific). After incubation for 8 min at 75°C to inactivate DNAse, 200 U M-MLV Reverse Transcriptase was added with subsequent

incubation at 25°C for 10 min and then at 37°C for 1 h. The reverse transcription reaction was terminated by heating at 95°C for 5 min and then chilling and storing at −80°C.

Real-time quantitative PCR was performed using the SsoFast™ EvaGreen® Supermix (Bio-Rad). Expression of each gene was studied and compared with that of the housekeeping gene encoding RPS29 (ribosomal protein 29). PCR was carried out in a 96-well format with 20-µl reactions containing SsoFast™ EvaGreen® Supermix (10 µl), cDNA (2 µl), gene-specific primers (0.5 µl) and DNase/RNase-free water (7 µl). Reactions entailed a standard two-step cycling program: 95°C for 3 s and 60°C for 30 s, for 40 cycles. mRNA levels were calculated relative to the average value obtained for the housekeeping gene and further normalized to the relative expression of the respective controls (*i.e.*, wild-type mice fed the CD diet).

2.6 – Analysis of plasma samples

Commercial colorimetric kits (Biolabo SA) based on the CHOD-PAP and GPO-PAP detection methods, coupling enzymatic reaction, and spectrophotometric detection of reaction end-products were used for determination of plasma triglycerides and cholesterol levels. Plasma ALT and AST were determined using a COBAS-MIRA+ biochemical analyzer (Anexplo facility, Toulouse, France).

Levels of cytokines [interleukin-6 (IL6), interleukin-10 (IL10), tumor-necrosis factor α (TNF- α), and monocyte chemoattractant protein 1 (MCP-1)] were assayed in mouse plasma samples collected by cardiac puncture upon euthanization; a Milliplex mouse cytokine magnetic kit (Millipore, France) was used according to the manufacturer's instructions. The inflammatory index was calculated as follows: for each mouse, the concentration value of each cytokine was expressed as the percentage of the mean concentration of the control CD group (set at 100%) The mean % (± SE) was then calculated for each animal and values were then divided by 100.

2.7 - Oral glucose tolerance test

After an overnight fast, mice were given an oral gavage glucose load (3 mg/g body wt). Blood glucose in samples obtained from the tail vein was assayed with a portable glucometer 30 min before oral glucose loading and at 0, 15, 30, 45, 60, 90 and 120 min thereafter. Insulin concentration in plasma (5 µl sample) was determined 30 min before and 15 min after glucose loading using an ELISA kit (Mercodia, Uppsala, Sweden).

2.8 – Analysis of insulin signaling

To analyze the liver insulin signaling pathway, mice received insulin at 1 mU / g body wt (Actrapid; Novo Nordisk) under anesthesia (ketamine, 100 mg/kg, Rompun, Bayer, France; and xylazine, 15 mg/kg, Imalgene 1000, Merial, France) into the portal vein. At 3 min post-injection, mice were euthanized and the liver rapidly dissected. Each individual mouse liver was homogenized using the Precellys lysing kit in RIPA buffer containing a protease inhibitor cocktail (leupeptin, aprotinin). Protein concentration in thawed samples (stored at –80°C) was measured using the Bradford method (Bio-Rad).

The percentage of phospho-Ser-473-Akt (pAkt) to total Akt was determined by capillary Western blot analysis using the ProteinSimple Wes System with 12- to 230-kDa Wes Separation Module capillary cartridges (ProteinSimple, Santa Clara, CA). A mouse monoclonal antibody specific for Akt (cat. no. 2920S, Cell Signaling) and rabbit polyclonal antibody specific for phosphorylated Akt (pAkt, Ser473, cat. no. 9271T, Cell Signaling) were used at a dilution of 1:100. Anti-mouse and anti-rabbit detection modules for Wes (ProteinSimple) kits included Luminol-S, peroxide, antibody diluent, streptavidin-coupled horseradish peroxidase, and anti-mouse and anti-rabbit secondary antibodies. Sample proteins (5 ng per each condition) were allowed to separate via the capillary technology and were analyzed based on chemiluminescence, which was transformed into digital images depicting bands as observed in Western blots. The abundance of each of total Akt and pAkt was determined using Compass software (ProteinSimple). The normalized data are expressed as the percentage of pAkt to total Akt.

2.9 - Statistical analysis

Data are expressed as the mean ± SE and analyzed using Prism V.5.01 for Windows (GraphPad Software, San Diego, CA). Data were examined for outliers using the Grubb's test and two outliers values were found in the whole study and excluded. Differences between groups were assessed using the Student's t-test or one-way analysis of variance followed by Bonferroni *post-hoc* test when necessary. The level of significance was defined as $p < 0.05$.

3 – RESULTS

3.1 - HFCC-CDX feeding for 1 wk causes hepatic steatosis and inflammation that is associated with systemic inflammation.

We first evaluated the ability of the HFCC-CDX diet to induce NASH features within 1 wk. C57BL6/J male mice (8 wk old) were divided into two groups and fed either a CD or HFCC-CDX diet for 1 wk. The livers of mice fed HFCC-CDX were grossly enlarged (30% increase in liver weight; Figure 1A) and pale in color (Figure 1B). Liver histological analyses were performed using ORO, H&E and Sirius red staining. ORO staining revealed lipid accumulation in the HFCC-CDX group as compared with the CD group (Figure 1B, ORO), and H&E staining revealed that the HFCC-CDX diet initiated infiltration of mononuclear inflammatory cells, which were absent in the CD-fed group (Figure 1B, H&E, white open circle). Fibrosis was detected in either groups (Figure 1B, SR). Given the apparently healthy liver phenotype of the CD group, an NAFLD activity score was calculated only for the HFCC-CDX group, and each score for steatosis and inflammation confirmed the histological observations (Figure 1C).

Analysis of hepatic lipid content revealed a twofold increase in hepatic triglycerides, cholesterol, and non-esterified fatty acids (NEFAs) as compared with the CD-fed group (Figure 1D), confirming the establishment of hepatic steatosis within 1 wk of HFCC-CDX feeding.

Hepatic cholesterol and free fatty acid overload induce oxidative stress that drives lipotoxicity and cellular injury, which are considered critical factors in NASH pathogenesis (29). We therefore analyzed whether the HFCC-CDX diet could induce hepatic oxidative stress and lipid peroxidation by measuring the production of ROS and TBARS, which are byproducts of lipid peroxidation (13). Both hepatic ROS and TBARS levels were significantly higher in the HFCC-CDX–fed group, with a 30% and 345% increase, respectively, compared with the CD group (Figure 1E and 1F). We further analyzed hepatic expression of candidate genes associated with NASH pathology. Confirming the inflammatory response to HFCCCDX feeding, expression of genes encoding inflammatory cytokines and macrophages chemotactic factors, including *TNF*α, *MCP-1*, *IL1*β, and *F4/80*, were significantly increased in HFCC-CDX mice compared with CD mice (Fig. 1*G*). Interestingly, the hepatic expression of certain genes related to fibrosis, e.g., collagen type 1 (*Col1α1*) and transforming growth factor *β* (*TGF β*), was also significantly increased in the HFCC-CDX group (Fig. 1*G*), suggesting that the fibroproliferative response was also activated.

We then analyzed NASH-related systemic effects. As anticipated, mice fed HFCC-CDX for 1 wk had a dyslipidemic profile, with 100% higher plasma triglycerides and 75% higher cholesterol levels compared with the CD mice (Figure 2A); also, the plasma levels of the transaminases ALT and AST aminotransferase were dramatically increased, reflecting liver injury (Figure 2B). Moreover, the HFCC-CDX mice had significantly higher levels of plasma inflammatory cytokines, including IL6

(+178%, $p < 0.05$) and MCP-1 (+160%, $p < 0.05$), and a trend toward higher IL10 (+30%) and TNF-α (+70%) was also observed (Figure 2C). Accordingly, the HFCC-CDX diet dramatically increased the inflammatory index based on differences in inflammatory cytokines levels between mice fed the CD diet or HFCC-CDX diet (Figure 2D).

Next, we found that HFCC-CDX feeding for 1 wk did not affect oral glucose tolerance (Figure 2E) and plasma insulin level (Figure 2F). However, direct liver stimulation via injection of insulin into the portal vein caused a significant reduction in phosphorylation of Akt at Ser473 in the HFCC-CDX group (Figure 2G), reflecting impaired insulin signaling. Phosphorylated Akt was not detectable in unstimulated groups. These results indicated that HFCC-CDX feeding for 1 wk established hepatic insulin resistance that had yet to translate into impaired whole body glucose metabolism. Overall, these data revealed that HFCC-CDX feeding for 1 wk is sufficient to induce some important NASH features, including hepatic steatosis and inflammation.

3.2 – Treatment with liraglutide partially reverses NASH features and reduces systemic inflammation and insulin resistance induced by the HFCC-CDX diet

To evaluate whether a longer-term dietary intervention could accentuate the NASH features that were observed after 1 wk of feeding of the HFCC-CDX diet (Figure 1 and 2), a group of mice was fed the diet for two additional weeks (HFCC-CDX group). In parallel, to assess the relevance of this dietary NASH model, we included another group fed the HFCC-CDX diet for 3 wk to assess whether once-daily treatment with liraglutide for the last 2 wk could confer protection against NASH [HFCC-CDX-Lira (liraglutide) group]. Liraglutide is a GLP-1 analog licensed for the treatment of type 2 diabetes and is currently in advanced clinical development for NASH (2, 14). Among all mice used in this experiment, one-third were fed the HFCC-CDX diet and injected with vehicle (phosphate-buffered saline; liraglutide control group) for the last 2 wk of feeding, and another third were fed the HFCC-CDX diet and injected with liraglutide. The remaining third comprised the control mice (no steatosis) that were fed the CD diet.

Total caloric intake was greater for the HFCC-CDX group compared with the CD group (Figure 3A), but there was no difference in body weight gain between these two groups throughout the feeding period (Figure 3B). As expected, however, liraglutide treatment reduced caloric intake, which was associated with body weight loss compared with non-treated mice (HFCC-CDX group, Figure 3A, B). Compared with HFCC-CDX feeding for 1 wk, the NASH phenotype continued to worsen at 3 wk, as

manifested by hepatomegaly (Figure 3C), fatty liver (Figure 3D), and increased content of hepatic triglycerides, cholesterol, and NEFAs (Figure 3E). Treatment with liraglutide significantly reduced liver weight and hepatic triglycerides to a level similar to that of the CD group, without modifying hepatic content of cholesterol and NEFAs.

Liver histology was performed (Figure 3F), and the NAFLD activity score was calculated for each of the HFCC-CDX and HFCC-CDX-Lira groups (Figure 3G); the total score comprised the sum of scores for each of hepatocellular steatosis, interstitial inflammation, and lobular fibrosis. For the HFCC-CDX group, steatosis ranged from score 2 limited to Zone 2 or 3 to a score-3 pan-lobular steatosis. The steatosis was solely microvesicular in appearance (Figure 3F, ORO). A maximal inflammation score of 3 was also observed for all animals fed the HFCC-CDX diet. Changes in inflammation were characterized by the presence of a large number of variably sized interstitial foci composed of mononuclear inflammatory cells (Figure 3F, H&E, open white circles). Finally, low score 2 perisinusoidal and periportal fibrosis was observed for all animals fed the HFCC-CDX diet (Figure 3F, Sirius Red, open black circles, and Figure 3G). In contrast, mice treated with liraglutide (HFCC-CDX-Lira group) had less extensive and less severe microvesicular steatosis and a reduced number of inflammation-associated mononuclear cells (Figure 3F, G). As with the vehicle-treated mice (HFCC-CDX group), a low score 2 periportal/perisinusoidal fibrosis was observed for all mice treated with liraglutide. Thus, mice treated with liraglutide had a lower total NAFLD activity score, mainly due to less extensive steatosis and inflammation.

Liver ROS and TBARS levels continued to increase following 3 wk of HFCC-CDX feeding and liraglutide treatment normalized to values obtained for the CD group (Figure 3H and I), indicating that hepatic oxidative stress and lipid peroxidation induced by HFCC-CDX feeding was resolved by liraglutide treatment.

The ongoing progression of NASH during the 3-wk HFCC-CDX diet was confirmed by the dramatic increase in the expression of genes encoding inflammatory cytokines and macrophages chemotactic factors, including *TNFα*, *MCP-1*, *IL1β* and *F4/80* compared with the CD group (Figure 3J). The differences in expression between the two groups were greater than those observed at 1 wk into the study period (Figure 1G). In line with the histological analyses of fibrosis, the expression of genes related to fibrosis [*Col1α1*, α-smooth muscle actin (α*SMA*), *TGFβ*, and tissue inhibitor of metalloproteinase 1 (*Timp1*)] were significantly greater in the HFCC-CDX group (Fig. 3*J*). Mice of the HFCC-CDX-Lira group had significantly lower expression of *IL1β*, *Col1α1*, and α*SMA* compared with

the HFCC-CDX group, whereas expression of *TNFα*, *MCP1*, *F4/80*, *TGFβ*, and *Timp1* was not affected by liraglutide treatment.

Concerning NASH-related systemic features, treatment of the HFCC-CDX mice with liraglutide normalized plasma triglyceride levels to those of the CD group, although liraglutide had no effect on the HFCC-CDX–induced hypercholesterolemia (Figure 4A) or on plasma transaminases (Figure 4B). The HFCC-CDX–induced increase in levels of plasma inflammatory cytokines was sustained after 3 wk of the dietary period, and liraglutide significantly reduced the levels of both IL6 and IL10 (Figure 4C), which translated into a significant reduction of the inflammatory index as compared with the non-treated HFCC-CDX group (Figure 4D). Concerning glucose metabolism, results of the oral glucose tolerance test did not differ between the HFCC-CDX and CD groups (Figure 4E), although the HFCC-CDX diet caused insulin resistance, as shown by the increased basal and glucose-stimulated insulin levels (Figure 4F), and impaired hepatic insulin signaling (Figure 4G). As expected, liraglutide treatment improved glucose tolerance (Figure 4E) and protected from HFCC-CDX–induced insulin resistance (Figure 4F and 4G).

4 - DISCUSSION

For purposes of preclinical assessment, we characterized and validated a novel dietary mouse model that recapitulates the major hallmarks of human NASH within 3 wk of the diet. In the proposed model, the C57BL/6 genetic background was chosen because it is more susceptible to liver injury than other inbred strains (28, 35, 36). The HFCC-CDX diet used in this model was formulated to be high in fat (60 kcal%), cholesterol (1.25%) and cholic acid (0.5%) and was supplemented with 2% CDX in drinking water. With this model, we had the objective of potentiating NASH development *via* the ability of cholic acid and CDX to stimulate the intestinal absorption of cholesterol and lipids and to increase hepatic cholesterol content and inflammation (7, 25, 37). The NASH features reproduced in this model include liver steatosis (characterized by excessive accumulation of triglycerides, cholesterol and NEFAs within the first week of the diet), a marked rise in the level of the liver-impairment marker ALT, oxidative stress, and hepatic inflammation and progression to mild fibrosis within 3 wk. This model also exhibited transcriptomic and metabolic alterations associated with the human disease, including insulin resistance, dyslipidemia, and systemic inflammation.

For a short period of dietary intervention (e.g., 3 wk in our study), none of the current diet-induced mouse models of NAFLD/NASH can recapitulate the human pathogenesis as well our HFCC-CDX model. For instance, feeding C57BL/6J mice a high fat (60% kcal) diet containing cholesterol (1.25%)

and cholate (0.5%) for 12 wk was found to induce steatosis, inflammation, and fibrosis associated with dyslipidemia, lipid peroxidation, oxidative stress, and insulin resistance (21), whereas we found that a similar NASH phenotype was induced in just 3 wk of feeding with the HFCC-CDX diet. Likewise, Western-type diets of varying composition with respect to fat (21–45 kcal%), cholesterol (0.1–2%), and sugars (e.g., 20% fructose) closely mimic the pathogenesis of human NASH, i.e., insulin resistance, inflammation and liver fibrosis; regardless of the composition, however, the NASH phenotype manifested only after a relatively long-term diet duration of 8 - 30 wk (14, 30). C57BL/6J mice fed a methionine- and choline-deficient diet develop a NASH phenotype in the shortest time compared with all previous NASH models, with hepatic steatosis by 2–4 wk and progression to inflammation and fibrosis shortly thereafter, although animals lose weight and do not develop insulin resistance (40, 41). In contrast, the present HFCC-CDX dietary model more closely recapitulates the NASH-associated metabolic dysfunctions of humans, including insulin resistance. One limitation of the HFCC-CDX dietary model for NASH compared to the disease development in humans is that mice do not become obese. Indeed, mice fed HFCC-CDX did not gain more weight than mice fed CD, despite an increase in total caloric intake. Energy expenditure was not measured in the present work. However, some studies have reported that high fat diet supplementation with 0.5% cholic acid counteracted the development of obesity in mice (38, 39). This effect was attributed to an increase in energy expenditure arising from an induction of brown adipose tissue thermogenesis. Thus, an elevation in energy expenditure in the HFCC-CDX group could explain the lack of body weight gain despite higher caloric intake compared to the CD group.

We also used our 3-wk HFCC-CDX dietary mouse model to test the therapeutic efficacy of liraglutide. Indeed, in addition to the attributes of improving glucose metabolism, reducing food intake, and promoting weight loss, certain other systemic and hepatic effects of liraglutide have been documented in preclinical and clinical studies; hence, liraglutide has been the subject of extensive evaluation as a therapeutic candidate for NAFLD (5, 16). Our present study revealed that once-daily injection of liraglutide for 2 wk decreased caloric intake and body weight, improved glucose tolerance, and protected from HFCC-CDX–induced insulin resistance, which are well-known effects of liraglutide in humans (5, 16). Additionally, we observed that liraglutide could resolve hypertriglyceridemia and reduce hepatic steatosis, oxidative stress, and systemic and hepatic inflammation but not fibrosis; these results are in general agreement with the effects of liraglutide documented in preclinical studies with mice (23, 24, 32) and clinical trials for NASH (11, 17, 18). In NAFLD patients, plasma ALT and

AST levels have been found to decrease gradually during liraglutide treatment (11, 17, 18). Indeed, in our experimental setting, liraglutide could significantly decrease the total NAFLD activity score but could not counter the HFCC-CDX–induced increase in plasma ALT and AST, AST; these results agree with those from another dietary mouse model of NASH (23). Whether longer-term treatment with liraglutide can reduce transaminase levels (as observed in human studies) and hepatic content in cholesterol and NEFAs (as reported in some animal models) (15, 33) will require a different experimental design. In this respect, the objective of the present work was to provide a preclinical model to facilitate rapid screening of therapeutic targets to treat NASH, but future studies must explore whether HFCC-CDX fed over a longer period might promote progression to more severe stages of NASH, such as advanced fibrosis, cirrhosis, and hepatocellular carcinoma. Additionally, we chose the mouse strain C57BL/6 based on its reasonable cost and susceptibility to diet-induced liver steatosis compared wither other inbred strains (28, 35, 36). Future studies could investigate the effect of the HFCC-CDX diet on isogenic strains selected for their susceptibility to develop diet-induced NASH or genetic mouse models that are predisposed to developing a fatty liver (3, 10, 33).

In summary, although drug-development research for NASH is intense and advancing rapidly, here we propose HFCC-CDX as a new dietary model of NASH that reproduces the main features of disease development in humans for the purpose of facilitating the rapid screening of drug candidates and prioritizing the more promising candidates for advanced preclinical assessment and subsequent clinical trials.

ACKNOWLEDGMENTS

The authors thank the following individuals for excellent technical assistance: the staff of the Rangueil animal facility (CREFRE, Toulouse), Lucie Fontaine (Histology core facility, I2MC, Toulouse), Alexandre Lucas (We-Met *Functional Biochemistry Facility*, I2MC, Toulouse) and Laurent Montbrun (ANEXPLO Phenotyping facility, CREFRE, Toulouse).

GRANTS

This work was supported by the French National Research Agency (ANR; Grant No ANR-16-CE18-0014-01) and the “Région Midi-Pyrénées - Occitanie” (CLE 2015, Grant No 14054132).

DISCLOSURES

F.B. and T.S. are employees of Physiogenex SAS. C.T is employee of Lifesearch SAS. None of the other authors has any conflicts of interest, financial or otherwise, to disclose.

AUTHOR CONTRIBUTIONS

T.D., F.B., T.S., and L.O.M. conceived and designed research; T.D., C.T., J.M., and G.C. performed experiments; T.D., F.B., S.N., and L.O.M. analyzed data; T.D. interpreted results of experiments; T.D. prepared figures; T.D. and L.O.M. drafted manuscript; T.D. and L.O.M. edited and revised manuscript; T.D., F.B., C.T., J.M., G.C., T.S., and L.O.M. approved final version of manuscript.

REFERENCES

1. **Angulo P**. Nonalcoholic fatty liver disease. *N Engl J Med* 346: 1221–21, 2002.
2. **Armstrong MJ**, **Gaunt P**, **Aithal GP**, **Barton D**, **Hull D**, **Parker R**, **Hazlehurst JM**, **Guo K**, **Abouda G**, **Aldersley MA**, **Stocken D**, **Gough SC**, **Tomlinson JW**, **Brown RM**, **Hübscher SG**, **Newsome PN**. Liraglutide safety and efficacy in patients with non-alcoholic steatohepatitis (LEAN): A multicentre, double-blind, randomised, placebo-controlled phase 2 study. *Lancet* 387: 679–690, 2016.
3. **Arsov T**, **Larter CZ**, **Nolan CJ**, **Petrovsky N**, **Goodnow CC**, **Teoh NC**, **Yeh MM**, **Farrell GC**. Adaptive failure to high-fat diet characterizes steatohepatitis in Alms1 mutant mice. *Biochem Biophys Res Commun* 342: 1152–1159, 2006.
4. **Ascha MS**, **Hanouneh IA**, **Lopez R**, **Tamimi TA-R**, **Feldstein AF**, **Zein NN**. The incidence and risk factors of hepatocellular carcinoma in patients with nonalcoholic steatohepatitis. *Hepatology* 51: 1972–1978, 2010.
5. **Buse JB**, **Rosenstock J**, **Sesti G**, **Schmidt WE**, **Montanya E**, **Brett JH**, **Zychma M**, **Blonde L**. Liraglutide once a day versus exenatide twice a day for type 2 diabetes: a 26-week randomised, parallel-group, multinational, open-label trial (LEAD-6). *Lancet* 374: 39–47, 2009.
6. **Chalasani N**, **Younossi Z**, **Lavine JE**, **Charlton M**, **Cusi K**, **Rinella M**, **Harrison SA**, **Brunt EM**, **Sanyal AJ**. The diagnosis and management of nonalcoholic fatty liver disease: Practice guidance from the American Association for the Study of Liver Diseases. *Hepatology* 67: 328–357, 2018.
7. **Christian A**, **Haynes MP**, **Phillips MCMCM**, **George H**, **Haynes MP**, **Phillips MCMCM**, **Rothblat GH**, **Christian AE**, **Haynes MP**, **Phillips MCMCM**, **Rothblat GH**. Use of cyclodextrins for manipulating cholesterol content. *J Lipid Res* 38: 2264–2272, 1997.
8. **Deng QG**, **She H**, **Cheng JH**, **French SW**, **Koop DR**, **Xiong S**, **Tsukamoto H**. Steatohepatitis induced by intragastric overfeeding in mice. *Hepatology* 42: 905–914, 2005.
9. **Estes C**, **Razavi H**, **Loomba R**, **Younossi Z**, **Sanyal AJ**. Modeling the epidemic of nonalcoholic fatty liver disease demonstrates an exponential increase in burden of disease. *Hepatology* 67: 123–133, 2018.
10. **Farrell GC**, **Mridha AR**, **Yeh MM**, **Arsov T**, **Van Rooyen DM**, **Brooling J**, **Nguyen T**, **Heydet D**, **Delghingaro-Augusto V**, **Nolan CJ**, **Shackel NA**, **Mclennan S V.**, **Teoh NC**, **Larter CZ**. Strain dependence of diet-induced NASH and liver fibrosis in obese mice is linked to diabetes and inflammatory phenotype. *Liver Int* 34: 1084–1093, 2014.
11. **Feng W**, **Gao C**, **Bi Y**, **Wu M**, **Li P**, **Shen S**, **Chen W**, **Yin T**, **Zhu D**. Randomized trial comparing the effects of gliclazide, liraglutide, and metformin on diabetes with non-alcoholic fatty liver disease. *J Diabetes* 9: 800–809, 2017.
12. **Folch J**, **Lees M**, **Stanley GHS**. A simple method for the isolation and purification of total lipids from animal tissues. *J Biol Chem* 226: 497–509, 1957.
13. **Fraga CG**, **Leibovitz BE**, **Tappel AL**, **Tissue IN**, **Fraga CG**, **Leibovitz BE**. Lipid peroxidation measured as thiobarbituric acid-reactive substances in tissue slices: characterization and comparison with homogenates and microsomes. *Free Radic Biol Med* 4: 155–161, 1988.
14. **Friedman SL**, **Neuschwander-Tetri BA**, **Rinella M**, **Sanyal AJ**. Mechanisms of NAFLD

development and therapeutic strategies. *Nat Med* 24: 908–922, 2018.
15. **Gao H**, **Zeng Z**, **Zhang H**, **Zhou X**, **Guan L**, **Deng W**, **Xu L**. The Glucagon-Like Peptide-1 Analogue Liraglutide Inhibits Oxidative Stress and Inflammatory Response in the Liver of Rats with Diet-Induced Non-alcoholic Fatty Liver Disease. *Biol Pharm Bull Pharm Bull* 38: 694–702, 2015.
16. **Garber A**, **Henry R**, **Ratner R**, **Garcia-Hernandez PA**, **Rodriguez-Pattzi H**, **Olvera-Alvarez I**, **Hale PM**, **Zdravkovic M**, **Bode B**. Liraglutide versus glimepiride monotherapy for type 2 diabetes (LEAD-3 Mono): a randomised, 52-week, phase III, double-blind, parallel-treatment trial. *Lancet* 373: 473–481, 2009.
17. **Gough SC**, **Yu J**, **Barton D**, **Guo K**, **Tomlinson JW**, **Newsome PN**, **Gathercole LL**, **Armstrong MJ**, **Hazlehurst JM**, **Nasiri M**, **Hull D**. Glucagon-like peptide 1 decreases lipotoxicity in non-alcoholic steatohepatitis. *J Hepatol* 64: 399–408, 2015.
18. **Khoo J**, **Hsiang J**, **Taneja R**, **Law NM**, **Ang TL**. Comparative effects of liraglutide 3 mg vs structured lifestyle modification on body weight, liver fat and liver function in obese patients with non-alcoholic fatty liver disease: A pilot randomized trial. *Diabetes, Obes Metab* 19: 1814–1817, 2017.
19. **Kleiner DE**, **Brunt EM**, **Van Natta M**, **Behling C**, **Contos MJ**, **Cummings OW**, **Ferrell LD**, **Liu YC**, **Torbenson MS**, **Unalp-Arida A**, **Yeh M**, **McCullough AJ**, **Sanyal AJ**. Design and validation of a histological scoring system for nonalcoholic fatty liver disease. *Hepatology* 41: 1313–1321, 2005.
20. **Machado MLVM**, **Diehl AM**. Animal models of nonalcoholic fatty liver disease. *Alcohol Non-Alcoholic Fat Liver Dis Bench to Bedside* 8: 121–145, 2015.
21. **Matsuzawa N**, **Takamura T**, **Kurita S**, **Misu H**, **Ota T**, **Ando H**, **Yokoyama M**, **Honda M**, **Zen Y**, **Nakanuma Y**, **Miyamoto KI**, **Kaneko S**, **Honda M**, **Kaneko S**, **Miyamoto KI**, **Yokoyama M**, **Ando H**, **Kurita S**, **Takamura T**, **Nakanuma Y**, **Misu H**, **Matsuzawa N**. Lipid-induced oxidative stress causes steatohepatitis in mice fed an atherogenic diet. *Hepatology* 46: 1392–1403, 2007.
22. **Mccullough AJ**. Epidemiology of the metabolic syndrome in the USA. *J. Dig. Dis.*: 333–340, 2011.
23. **Mells JE**, **Fu PP**, **Sharma S**, **Olson D**, **Cheng L**, **Handy JA**, **Saxena NK**, **Sorescu D**, **Anania FA**. Glp-1 analog, liraglutide, ameliorates hepatic steatosis and cardiac hypertrophy in C57BL/6J mice fed a Western diet. *AJP Gastrointest Liver Physiol* 302: G225–G235, 2012.
24. **Moreira G V.**, **Azevedo FF**, **Ribeiro LM**, **Santos A**, **Guadagnini D**, **Gama P**, **Liberti EA**, **Saad MJA**, **Carvalho CRO**. Liraglutide modulates gut microbiota and reduces NAFLD in obese mice. *J Nutr Biochem* 62: 143–154, 2018.
25. **Murphy C**, **Parini P**, **Wang J**, **Björkhem I**, **Eggertsen G**, **Gåfvels M**. Cholic acid as key regulator of cholesterol synthesis, intestinal absorption and hepatic storage in mice. *Biochim Biophys Acta - Mol Cell Biol Lipids* 1735: 167–175, 2005.
26. **Sanches SCL**, **Ramalho LNZ**, **Augusto MJ**, **Da Silva DM**, **Ramalho FS**. Nonalcoholic Steatohepatitis: A Search for Factual Animal Models. *Biomed Res Int* 2015: 574–582, 2015.
27. **Santhekadur PK**, **Kumar DP**, **Sanyal AJ**. Preclinical models of non-alcoholic fatty liver disease. *J Hepatol* 68: 230–237, 2018.
28. **Shpyleva S**, **Pogribna M**, **Cozart C**, **Bryant MS**, **Muskhelishvili L**, **Tryndyak VP**, **Ross SA**, **Beland FA**, **Pogribny IP**. Interstrain differences in the progression of nonalcoholic steatohepatitis to fibrosis in mice are associated with altered hepatic iron metabolism. *J Nutr Biochem* 25: 1235–1242, 2014.
29. **Spahis S**, **Delvin E**, **Borys J-M**, **Levy E**. Oxidative Stress as a Critical Factor in Nonalcoholic Fatty Liver Disease Pathogenesis. *Antioxid Redox Signal* 26: 519–541, 2016.
30. **Stephenson K**, **Kennedy L**, **Hargrove L**, **Demieville J**, **Thomson J**, **Alpini G**, **Francis H**. Updates on dietary models of nonalcoholic fatty liver disease: Current studies and insights. *Gene Expr.* 18: 5–17, 2018.
31. **Szabados E**, **Fischer GM**, **Toth K**, **Csete B**, **Nemeti B**, **Trombitas K**, **Habon T**, **Endrei D**, **Sumegi B**. Role of reactive oxygen species and poly-ADP-ribose polymerase in the development of AZT-induced cardiomyopathy in rat [Online]. *Free Radic Biol …* 26: 309–317, 1999. http://www.ncbi.nlm.nih.gov/pubmed/9895221 [2 Dec. 2014].
32. **Tølbøl KS**, **Kristiansen MNNB**, **Hansen HH**, **Veidal SS**, **Rigbolt KTTG**, **Gillum MP**, **Jelsing J**, **Vrang N**, **Feigh M**, **Kristiansen MNNB**, **Jelsing J**, **Gillum MP**, **Tølbøl KS**, **Feigh M**, **Hansen HH**. Metabolic and hepatic effects of liraglutide, obeticholic acid and elafibranor in diet-induced obese mouse models of biopsy-confirmed nonalcoholic steatohepatitis. *World J Gastroenterol* 24: 179–194, 2018.
33. **Trak-Smayra V**, **Paradis V**, **Massart J**, **Nasser S**, **Jebara V**, **Fromenty B**. Pathology of the liver in obese and diabetic ob/ob and db/db mice fed a standard or high-calorie diet. *Int J Exp*

Pathol 92: 413–421, 2011.
34. **Traussnigg S**, **Kienbacher C**, **Halilbasic E**, **Rechling C**, **Kazemi-Shirazi L**, **Hofer H**, **Munda P**, **Trauner M**. Challenges and Management of Liver Cirrhosis: Practical Issues in the Therapy of Patients with Cirrhosis due to NAFLD and NASH. *Dig Dis* 33: 598–607, 2015.
35. **Tryndyak V**, **De Conti A**, **Kobets T**, **Kutanzi K**, **Koturbash I**, **Han T**, **Fuscoe JC**, **Latendresse JR**, **Melnyk S**, **Shymonyak S**, **Collins L**, **Ross SA**, **Rusyn I**, **Beland FA**, **Pogribny IP**. Interstrain differences in the severity of liver injury induced by a choline- and folate-deficient diet in mice are associated with dysregulation of genes involved in lipid metabolism. *FASEB J* 26: 4592–4602, 2012.
36. **Tsuchiya M**, **Ji C**, **Kosyk O**, **Shymonyak S**, **Melnyk S**, **Kono H**, **Tryndyak V**, **Muskhelishvili L**, **Pogribny IP**, **Kaplowitz N**, **Rusyn I**. Interstrain differences in liver injury and one-carbon metabolism in alcohol-fed mice. *Hepatology* 56: 130–139, 2012.
37. **Vergnes L**, **Phan J**, **Strauss M**, **Tafuri S**, **Reue K**. Cholesterol and Cholate Components of an Atherogenic Diet Induce Distinct Stages of Hepatic Inflammatory Gene Expression. *J Biol Chem* 278: 42774–42784, 2003.
38. **Watanabe M**, **Horai Y**, **Houten SM**, **Morimoto K**, **Sugizaki T**, **Arita E**, **Mataki C**, **Sato H**, **Tanigawara Y**, **Schoonjans K**, **Itoh H**, **Auwerx J**. Lowering bile acid pool size with a synthetic farnesoid X receptor (FXR) agonist induces obesity and diabetes through reduced energy expenditure. *J Biol Chem* 286: 26913–26920, 2011.
39. **Watanabe M**, **Houten SM**, **Mataki C**, **Christoffolete MA**, **Kim BW**, **Sato H**, **Messaddeq N**, **Harney JW**, **Ezaki O**, **Kodama T**, **Schoonjans K**, **Bianco AC**, **Auwerx J**. Bile acids induce energy expenditure by promoting intracellular thyroid hormone activation. *Nature* 439: 484–489, 2006.
40. **Weltman MD**, **Farrell GC**, **Liddle C**. Increased hepatocyte CYP2E1 expression in a rat nutritional model of hepatic steatosis with inflammation. *Gastroenterology* 111: 1645–1653, 1996.
41. **Yu Y**, **Liu Y**, **An W**, **Song J**, **Zhang Y**, **Zhao X**. STING-mediated inflammation in Kupffer cells contributes to progression of nonalcoholic steatohepatitis. *J Clin Invest* 129: 546–555, 2019.

FIGURE LEGENDS

Figure 1: Diet high in fat (60%), cholesterol (1.25%), and cholic acid (0.5%) along with 2% hydroxypropyl-β-cyclodextrin in drinking water (HFCC-CDX diet) for 1 wk induces liver steatosis, oxidative stress, and inflammation.

A) Liver weight. **B)** Representative photographs of macroscopic liver aspect, Oil Red O, hematoxylin and eosin (H&E), and Sirius Red staining in mice fed a HFCC-CDX or chow diet (CD) for 1 wk (magnification x20). White circles indicate the mononuclear-cell infiltrate (inflammation). **C)** Nonalcoholic fatty liver disease (NAFLD) activity score for mice fed HFCC-CDX. **D–F)** Assessment of hepatic triglycerides, cholesterol, and non-esterified fatty acids (NEFAs) (D), reactive oxygen species (ROS, E), and thiobarbituric acid response substrates (TBARS, F). **G)** Expression of proinflammatory genes [interleukin-1β (*IL1β*), tumor-necrosis factor α (*TNF α*), monocyte chemoattractant protein 1 (*MCP1*), and *F4/80*] and profibrotic genes [collagen type 1*α*1 (*Col1α1*), α-smooth muscle actin (*αSMA*), transforming growth factor β (*TGFβ*), and tissue inhibitor of metalloproteinase 1 (*Timp1*)] in liver. Open circles: CD; closed circles: HFCC-CDX diet. Results are presented as the mean ± SE, and the statistical significance of differences was determined with the Student's *t* test. **P* > 0.05, †*P* >0.01,

‡*P* > 0.001; ns, not significant. All data were obtained with 8-wk-old mice fed the HFCC-CDX or CD for 1 wk, *n* >10 mice per group

Figure 2: Increase in plasma lipids, systemic inflammation, and altered liver insulin sensitivity after 1 wk of feeding mice the diet high in fat (60%), cholesterol (1.25%), and cholic acid (0.5%) along with 2% hydroxypropyl- β -cyclodextrin in drinking water (HFCC-CDX diet).

A) Plasma triglycerides and cholesterol levels. **B)** Plasma alanine (ALT) and aspartate (AST) levels. **C)** Plasma concentrations of the inflammatory cytokines interleukin-6 (IL6), interleukin-10 (IL10), monocyte chemoattractant protein 1 (MCP1), and tumor-necrosis factor α (TNFα). **D)** Index of systemic inflammation based on differences in inflammatory cytokine levels between mice fed the chow diet (CD) or HFCC-CDX diet. AU, arbitrary units. **E)** Blood glucose evolution after oral glucose loading (oral glucose tolerance test, OGTT) in overnight-fasted mice. **F)** OGTT-associated basal and stimulated insulinemia values in overnight-fasted mice. **G)** Representative Western blot of total and phosphorylated Akt (P-Akt) levels in the liver of mice after portal PBS or insulin injection. Data are expressed as the percentage of P-Akt to total Akt. Open circles: CD; closed circles: HFCC-CDX diet. Results are presented as the mean ± SE, and the statistical significance of differences was determined with the Student's *t* test. **P* > 0.05,

Figure 3: Partial reversion of liver nonalcoholic fatty liver disease (NAFLD)/nonalcoholic steatohepatitis (NASH) features with 2 wk of treatment with liraglutide.

A) Total caloric intake. **B)** Body weight evolution. **C)** Final liver weight at euthanization. **D)** Representative photographs of dissected livers at euthanization. **E)** Content of triglycerides, cholesterol, and nonesterified fatty acids (NEFAs) in livers at euthanization. **F)** Representative images of the histological analysis of livers via staining with Oil Red O, hematoxylin and eosin (H&E), and Sirius Red for mice fed the chow diet (CD) or diet high in fat (60%), cholesterol (1.25%), and cholic acid (0.5%) along with 2% hydroxypropyl-β-cyclodextrin in drinking water (HFCC-CDX diet) and HFCC-CDX-fed mice treated with liraglutide (HFCC-CDX Lira; magnification x20). White circles indicate the mononuclear cell-infiltrate (inflammation), and black circles indicate collagen deposition (fibrosis). **G)** NAFLD activity score based on the results of staining of liver sections from HFCC-CDX and HFCC-CDX-Lira mice. **H)** Hepatic reactive oxygen species (ROS) levels. **I)** Hepatic thiobarbituric acid response substrates (TBARS) measurement. **G)** Liver expression of the proinflammatory genes interleukin-1β (*IL1β*), tumor-necrosis factor α (*TNFα*), monocyte chemoattractant protein 1 (*MCP1*),

and *F4/80* and profibrotic genes collagen type 1α1 (*Col1α1*), α-smooth muscle actin (*αSMA*), transforming growth factor β (*TGFβ*), and tissue inhibitor of metalloproteinase 1 (*Timp1*). White circles: CD; black circles: HFCC-CDX diet; gray circles: HFCC-CDX Lira. Results are presented as the mean±SE, and the statistical significance of differences was determined with the Student's *t* test or with one-way analysis of variance followed by Bonferroni's post hoc test. **P* > 0.05, †*P* > 0.01, ‡*P* > 0.001; ns, not significant. All data were obtained with 8-wk-old mice fed a CD or HFCC-CDX for 3 wk. HFCC-CDX-fed mice were treated daily with liraglutide or vehicle for the last 2 wk of the study, *n* >10 mice per group.

Figure 4: Liraglutide treatment normalizes both plasma lipid levels and systemic inflammation and improves insulin sensitivity.

A) Plasma triglycerides and cholesterol levels. **B)** Plasma alanine (ALT) and aspartate (AST) levels. **C)** Plasma concentrations of the inflammatory cytokines interleukin-6 (IL6), interleukin-10 (IL10), monocyte chemoattractant protein 1 (MCP1), and tumor-necrosis factor α (TNFα). **D)** Index of systemic inflammation. AU, arbitrary units. **E)** Blood glucose evolution after oral glucose loading (OGTT) in overnight-fasted mice. **F)** OGTT-associated basal and stimulated insulinemia values in overnight-fasted mice. **G)** Representative Western blot of total and phosphorylated Akt (P-Akt) levels in the liver of mice after portal insulin injection. Data are expressed as the percentage of (P-Akt) to total Akt. White circles: chow diet (CD); black circles: diet high in fat (60%), cholesterol (1.25%), and cholic acid (0.5%) along with 2% hydroxypropyl-β-cyclodextrin in drinking water (HFCC-CDX diet); gray circles: HFCC-CDX with liraglutide (HFCC-CDX Lira). Results are presented as the mean ± SE, and the statistical significance of differences were determined with one-way analysis of variance followed by Bonferroni's post hoc test. **P* >0.05, †*P* > 0.01, ‡*P* > 0.001; ns, not significant. All data were obtained with 8-wk-old mice fed the CD or HFCC-CDX diet for 3 wk. HFCC-CDX-fed mice were treated daily with liraglutide (HFCC-CDX-Lira) or vehicle (HFCC-CDX) for the last 2 wk of the study, *n* >10 mice per group.

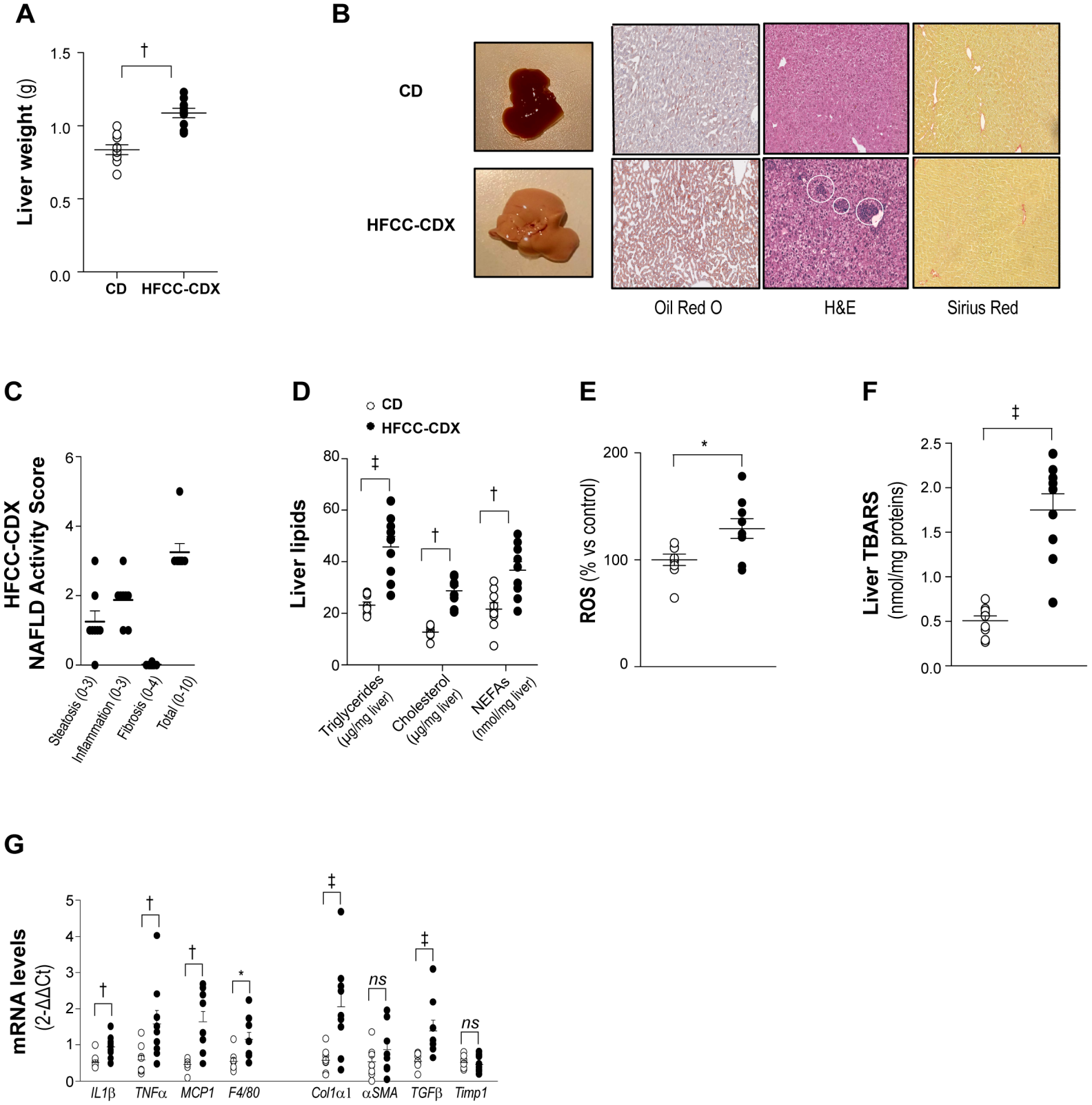
A
Liver weight (g)
1.5
1.0
0.5
0.0
†
CD
HFCC-CDX
B
CD
HFCC-CDX
Oil Red O
H&E
Sirius Red
C
HFCC-CDX
NAFLD Activity Score
6
4
2
0
Steatosis (0-3)
Inflammation (0-3)
Fibrosis (0-4)
Total (0-10)
D
CD
HFCC-CDX
Liver lipids
80
60
40
20
0
‡
†
†
Triglycerides (µg/mg liver)
Cholesterol (µg/mg liver)
NEFAs (nmol/mg liver)
E
ROS (% vs control)
200
100
0
*
F
Liver TBARS
(nmol/mg proteins)
2.5
2.0
1.5
1.0
0.5
0.0
‡
G
mRNA levels
(2-ΔΔCt)
5
4
3
2
1
0
†
†
†
*
‡
ns
‡
ns
IL1β
TNFα
MCP1
F4/80
Col1α1
αSMA
TGFβ
Timp1

Figure 1

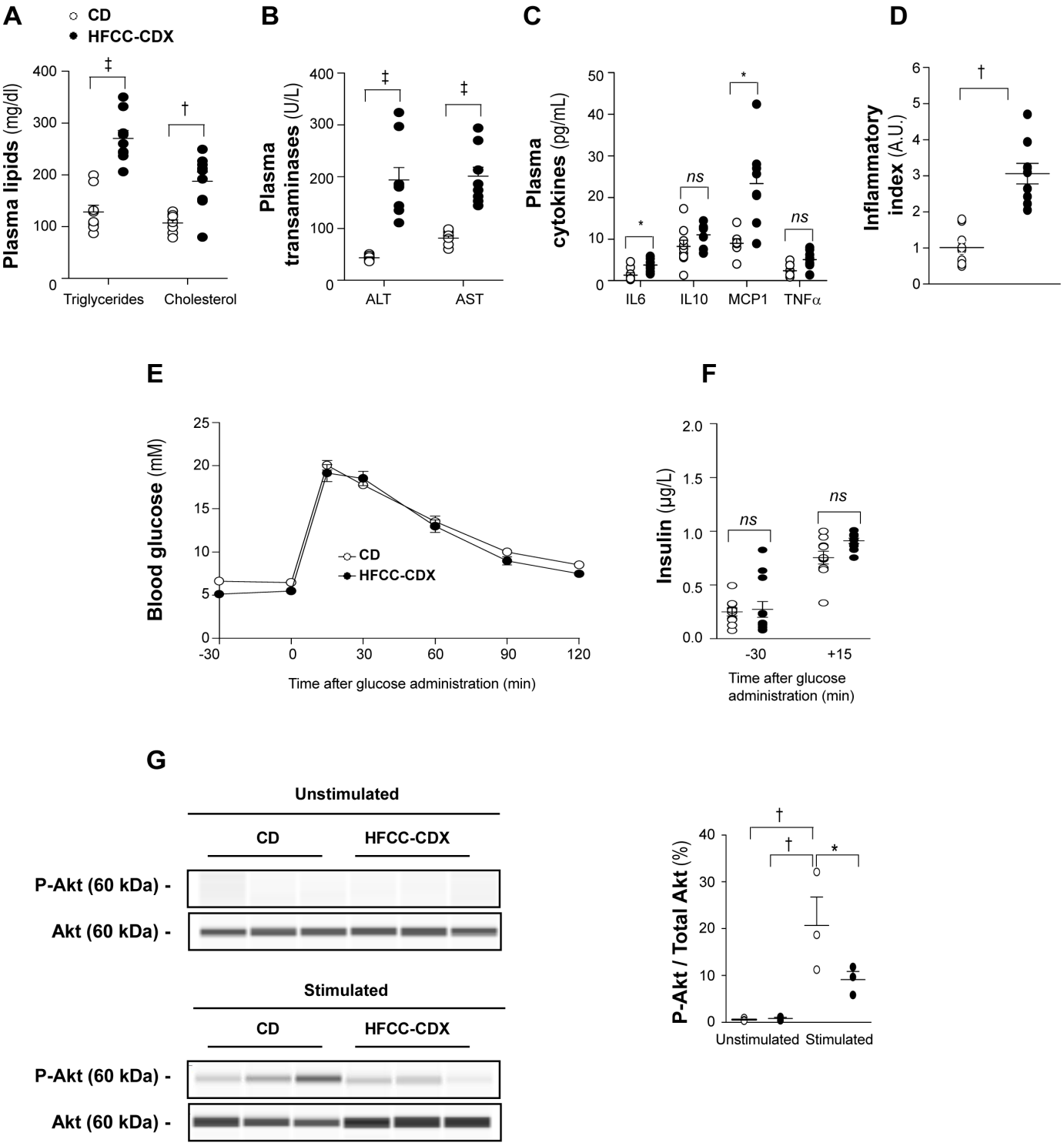
A
CD
HFCC-CDX
Plasma lipids (mg/dl)
Triglycerides
Cholesterol
B
Plasma transaminases (U/L)
ALT
AST
C
Plasma cytokines (pg/mL)
IL6
IL10
MCP1
TNFα
ns
D
Inflammatory index (A.U.)
E
Blood glucose (mM)
Time after glucose administration (min)
F
Insulin (µg/L)
Time after glucose administration (min)
G
Unstimulated
Stimulated
P-Akt (60 kDa) -
Akt (60 kDa) -
P-Akt / Total Akt (%)

Figure 2

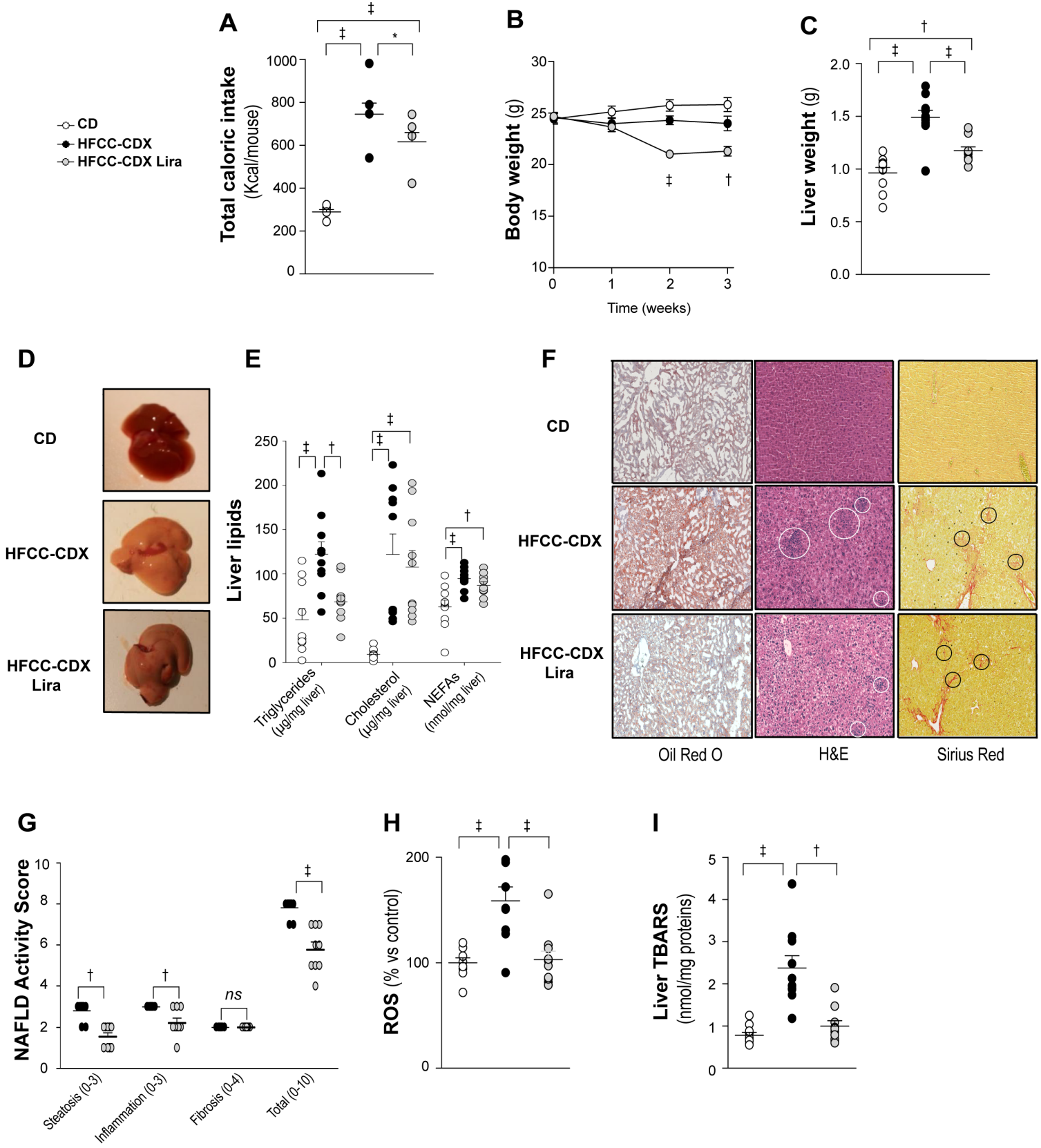
CD
HFCC-CDX
HFCC-CDX Lira
A
Total caloric intake (Kcal/mouse)
B
Body weight (g)
Time (weeks)
C
Liver weight (g)
D
CD
HFCC-CDX
HFCC-CDX Lira
E
Liver lipids
Triglycerides (µg/mg liver)
Cholesterol (µg/mg liver)
NEFAs (nmol/mg liver)
F
CD
HFCC-CDX
HFCC-CDX Lira
Oil Red O
H&E
Sirius Red
G
NAFLD Activity Score
Steatosis (0-3)
Inflammation (0-3)
Fibrosis (0-4)
Total (0-10)
ns
H
ROS (% vs control)
I
Liver TBARS (nmol/mg proteins)

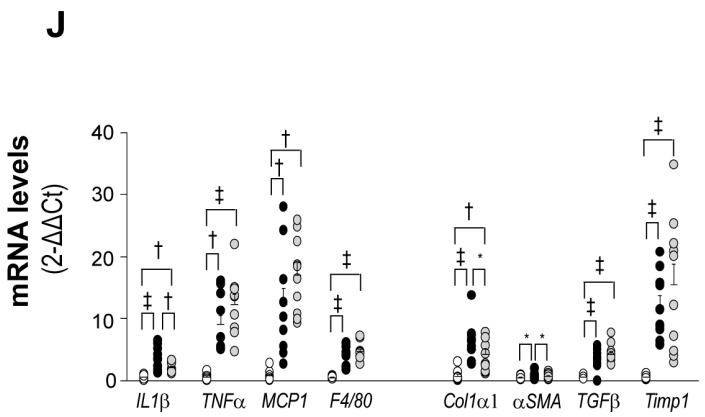
J
mRNA levels (2-ΔΔCt)
IL1β
TNFα
MCP1
F4/80
Col1α1
αSMA
TGFβ
Timp1

Figure 3

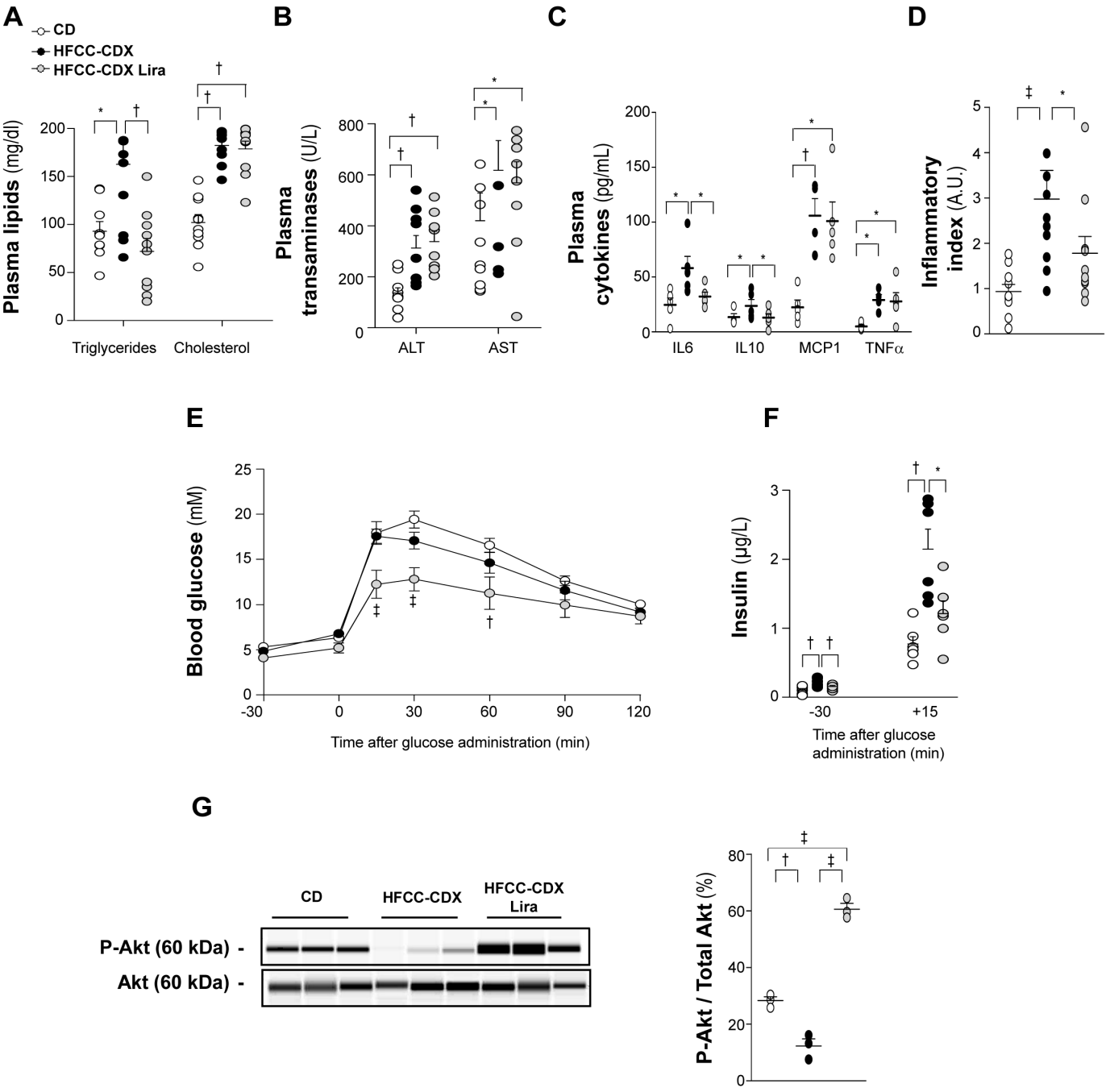
A
CD
HFCC-CDX
HFCC-CDX Lira
Plasma lipids (mg/dl)
Triglycerides
Cholesterol
B
Plasma transaminases (U/L)
ALT
AST
C
Plasma cytokines (pg/mL)
IL6
IL10
MCP1
TNFα
D
Inflammatory index (A.U.)
E
Blood glucose (mM)
Time after glucose administration (min)
F
Insulin (µg/L)
Time after glucose administration (min)
G
CD
HFCC-CDX
HFCC-CDX Lira
P-Akt (60 kDa) -
Akt (60 kDa) -
P-Akt / Total Akt (%)

Figure 4